

Coherent network analysis technique for discriminating gravitational-wave bursts from instrumental noise

Shourov Chatterji, Albert Lazzarini, Leo Stein, and Patrick J. Sutton
LIGO - California Institute of Technology, Pasadena, CA 91125

Antony Searle
Australian National University, Canberra, ACT 0200, Australia

Massimo Tinto
Jet Propulsion Laboratory, California Institute of Technology, Pasadena, CA 91109
 (Dated: October 30, 2018)

Existing coherent network analysis techniques for detecting gravitational-wave bursts simultaneously test data from multiple observatories for consistency with the expected properties of the signals. These techniques assume the output of the detector network to be the sum of a stationary Gaussian noise process and a gravitational-wave signal, and they may fail in the presence of transient non-stationarities, which are common in real detectors. In order to address this problem we introduce a consistency test that is robust against noise non-stationarities and allows one to distinguish between gravitational-wave bursts and noise transients. This technique does not require any *a priori* knowledge of the putative burst waveform.

PACS numbers: 04.80.Nn, 95.55.Ym, 07.05.Kf
 Keywords: Gravitational Waves, Laser Interferometry

I. INTRODUCTION

Gravitational-wave bursts (GWBs) are among the most exciting classes of signals that large-scale, broadband interferometric gravitational-wave observatories will attempt to detect. These instruments have already started to collect data, and are beginning to coordinate their activities in order to perform joint, world-wide, searches. The United States LIGO [1] observatory has reached its design sensitivity goal, and is currently conducting its fifth data-taking run. Both the British-German GEO600 [2] interferometer and the Japanese TAMA [3] detector have conducted multiple data-taking runs, often in coincidence with LIGO. The French-Italian VIRGO [4] detector is approaching its operational phase with an anticipated sensitivity comparable to that of the US detectors.

Potential sources of GWBs include merging compact objects [5, 6, 7], core-collapse supernovae [8, 9, 10, 11], and gamma-ray burst engines [12]. By considering the anticipated strengths of the gravitational-wave bursts emitted by these systems and the present performance of the detectors, it is clear that coincident experiments are necessary to maximize the chances of successfully identifying an astronomical event. This is because signals emitted by these sources cannot currently be modeled with sufficient accuracy to distinguish them from transient noise non-stationarities (“glitches”) affecting the data of the detectors. In addition, a real burst signal may not be much larger than the noise levels in the detectors. More detectors at the same site provide one way for increasing the signal-to-noise ratio (SNR), but a network of detectors spaced across the globe inherently provides much more information about the wave and its source. With

a network of three or more interferometers, for instance, one has in principle sufficient information for good SNRs to infer the direction to the source. If the events are not corroborated by an electromagnetic detection (optical, X-ray, or radio) this could be crucial. Such a network also has enough information to reconstruct the two independent polarization amplitudes of the wave. This is possible because three interferometers provide three independent measures of the gravitational wave (which are functions of time) and two independent time delays. If we consider the geometrical plane passing through the three sites of the interferometers, the two independent time delays jointly identify two possible points in the sky where the signal could have come from that are mirror-images of each other with respect to this plane; see Figure 1. Since the detector antenna patterns are not symmetric with respect to this plane, it is further possible to resolve this two-fold ambiguity by properly accounting for the antenna pattern asymmetry in the analysis of the data. Once the sky position has been determined it is straightforward to make a minimum-variance estimate of the two polarization waveforms of the GWB as linear combinations of the detector data streams. The extraction of this information from the combined responses of the individual detectors of the network is called the “solution of the inverse problem” in gravitational-wave astronomy.

The inverse problem for gravitational-wave bursts with a network of three wide-band, widely separated detectors was first solved by Gürsel and Tinto [13]. Their technique, which is referred to in recent literature as the *null-stream* method, relies on the observation that a gravitational-wave burst present in the data of a network of three wide-band detectors must satisfy a unique closure condition. Gürsel and Tinto studied a two-

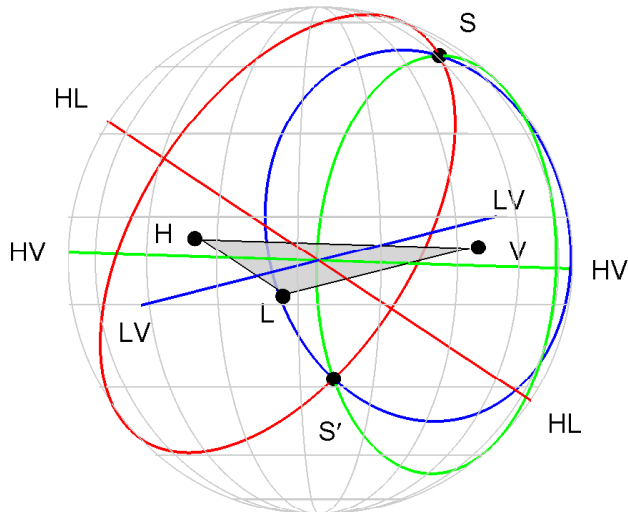


FIG. 1: Geometry of the network and travel times spent by a GWB to propagate across a three-detector network (detectors “H”, “L”, and “V”). The locus of constant time delay between two detectors form a ring on the sky concentric about the baseline between the two sites. For three detectors, these rings may intersect in two locations. One is the true source direction, S , while the other (S') is its mirror image with respect to the geometrical plane passing through the three sites. This two-fold ambiguity can be resolved by further considering the amplitudes of the responses. For four or more detectors there is a unique intersection point of all of the rings.

parameter family of linear combinations of the three data sets, in which the two parameters correspond to the two angular coordinates of the hypothesized sky location of the source. They showed that when the two parameters coincide with the true location of the source then the gravitational-wave burst is canceled precisely in the linear combination. This point is located by applying a least-squares minimization (i.e., a χ^2 test) to the linear combination. In [13] it was also shown that this condition holds regardless of the time dependence of the two polarization waveforms of the burst. This remarkable result makes this method very powerful for solving the inverse problem since it does not require *a priori* knowledge of the burst waveforms.

Even with the Gürsel-Tinto technique, lack of knowledge of the signal waveforms presents a serious impediment in searches for GWBs. This is because gravitational-wave detectors exhibit transient noise fluctuations, or “glitches”. Without a model for GWB waveforms, it is not obvious how to determine with confidence whether a candidate detection is a real gravitational-wave burst signal or a “false alarm” due to noise fluctuations occurring in coincidence in the detectors of the network. A confident detection of gravitational-wave bursts requires the ability to distinguish them from such noise transients. In this context, as pointed out in [14, 15, 16], the null-stream method could also be used

for discriminating gravitational-wave bursts from noise-triggered fluctuations affecting the data of the detectors. Put simply, uncorrelated noise glitches should not cancel in the null stream. In principle, therefore, they can be vetoed by setting a threshold on the maximum allowable χ^2 value. In practice, however, a χ^2 veto test is vulnerable to effects that prevent precise cancellation of strong GWBs, such as calibration errors, and may be ineffective for weak glitches, for which there are often sky positions which yield $\chi^2 \sim 1$ per degree of freedom even though the glitches are uncorrelated. A χ^2 threshold which is low enough to pass a GWB with poor data calibration may also pass a weak glitch. A χ^2 threshold which is high enough to reject the glitch may also reject the GWB.

In this paper we propose a modified null-stream based technique for discriminating GWBs from noise glitches. This technique is based on comparing the energy in the null stream to that expected if the transients in the detectors are uncorrelated. This second energy measure, which we call the *incoherent energy*, provides an effective measure of the significance of the χ^2 test and renders it robust against both calibration uncertainties and weak glitches. Like the Gürsel-Tinto analysis for determining the source direction, our null-stream consistency test does not require any *a priori* knowledge of the GWB (or glitch) waveforms.

Our paper is organized as follows. In Section II we show that there exists a very general and elegant procedure for deriving the null stream for an arbitrary number of detectors with colored noise. We then address the issue that the null-stream χ^2 alone can not reliably distinguish between a gravitational-wave burst and noise-generated glitches. This is done by introducing a complementary energy measure, the incoherent energy, and demonstrating that GWBs and glitches separate in the two-dimensional space of null and incoherent energies. This allows us to identify (or “veto”) noise-generated events and hence make the null-stream analysis robust against glitches.

In Section III we discuss the results of the numerical simulation of our statistical test applied to the LIGO-Virgo 3-detector network. We assume the three interferometers to be working at the LIGO design sensitivity, and quantify the ability of our method to distinguish true GWBs from coincident noise glitches. Although our numerical implementation is not optimized for the signals under consideration, it indicates that gravitational-wave bursts observed in each detector with SNRs of about 10 – 20 can reliably be distinguished from noise glitches of similar energy, and that a significant improvement over the statistics based on the null-stream χ^2 alone is achieved. Our conclusions and future work plans are presented in Section IV.

II. ANALYSIS

Three or more detectors provide redundant measurements of the two polarization components h_+ , h_\times of a gravitational wave. It is therefore possible to construct linear combinations of the data streams that do not contain any gravitational-wave component, i.e., that consist only of detector noise. In this section we derive these linear combinations, known as “null streams,” for networks containing an arbitrary number of detectors whose noises are different and colored.

A. Conventions

The conventions used for the notation in this report are described in Table I.

For a plane [32] gravitational wave incident from a direction $\hat{\Omega}_s$ the strain $h_{+,\times}$ at the position \vec{r}_α is related to that at some (arbitrary) reference position \vec{r}_0 by

$$h_{+,\times}(t + \Delta t_\alpha(\hat{\Omega}_s), \vec{r}_\alpha) = h_{+,\times}(t, \vec{r}_0), \quad (1)$$

where the time delay $\Delta t_\alpha(\hat{\Omega}_s)$ is given by

$$\Delta t_\alpha(\hat{\Omega}_s) \equiv \frac{1}{c}(\vec{r}_0 - \vec{r}_\alpha) \cdot \hat{\Omega}_s. \quad (2)$$

We can therefore compare the gravitational-wave signals measured by detectors at different locations by shifting the time-series data from each detector according to (2), provided we know the sky location of the source.

The time-series signal produced in detector α at \vec{r}_α by a gravitational-wave $h_{+,\times}$ incident from a sky position $\hat{\Omega}_s$ is

$$d_\alpha(t + \Delta t_\alpha(\hat{\Omega}_s)) = F_\alpha^+(\hat{\Omega}_s)h_+(t) + F_\alpha^\times(\hat{\Omega}_s)h_\times(t) + n_\alpha(t + \Delta t_\alpha(\hat{\Omega}_s)). \quad (3)$$

Here n_α is the stationary background noise of detector α as a function of time, calibrated to units of strain, and F_α^+ , F_α^\times are the antenna response functions [13] for detector α for the sky position $\hat{\Omega}_s$ of the gravitational wave source. For brevity, we write $h_{+,\times}(t) \equiv h_{+,\times}(t, \vec{r}_0)$.

B. Null stream construction

Let us assume for the moment that we know the direction $\hat{\Omega}_s$ to the source. Then we can time-shift the data from each detector as in (3), and drop explicit references to the time delays Δt_α and the sky position. Transforming to the Fourier domain, equation (3) becomes

$$\tilde{d}_\alpha(f) = F_\alpha^+ \tilde{h}_+(f) + F_\alpha^\times \tilde{h}_\times(f) + \tilde{n}_\alpha(f), \quad (4)$$

The Fourier transform and its inverse are defined by

$$\begin{aligned} \tilde{d}_\alpha(f) &= \int_{-\infty}^{+\infty} d_\alpha(t) e^{-2\pi i f t} dt, \\ d_\alpha(t) &= \int_{-\infty}^{+\infty} \tilde{d}_\alpha(f) e^{2\pi i f t} df. \end{aligned} \quad (5)$$

The one-sided strain noise power spectral density $S_\alpha(f)$ of the stationary noise n_α is given by

$$\langle \tilde{n}_\alpha(f) \tilde{n}_\beta^*(f') \rangle = \frac{1}{2} \delta_{\alpha\beta} \delta(f - f') S_\alpha(f). \quad (6)$$

For present detectors $S_\alpha(f)$ is a strongly varying function of frequency. Since it will prove convenient to work with white-noise data, without loss of generality we divide the strain data at each frequency by the estimated amplitude spectrum $\sqrt{S_\alpha(f)}/2$ of the corresponding detector noise. The whitened data $\tilde{d}_{w\alpha}$ is then given by

$$\begin{aligned} \tilde{d}_{w\alpha}(f) &\equiv \frac{\tilde{d}_\alpha(f)}{\sqrt{S_\alpha(f)}/2} \\ &= F_{w\alpha}^+ \tilde{h}_+(f) + F_{w\alpha}^\times \tilde{h}_\times(f) + \tilde{n}_{w\alpha}(f), \end{aligned} \quad (7)$$

where the $n_{w\alpha}(t)$ are unit Gaussian noise processes and $F_{w\alpha}^{+,\times}$ are the noise-weighted antenna responses

$$F_{w\alpha}^{+,\times}(\hat{\Omega}_s, f) \equiv \frac{F_\alpha^{+,\times}(\hat{\Omega}_s)}{\sqrt{S_\alpha(f)}/2}. \quad (8)$$

The $F_{w\alpha}^{+,\times}$ contain all of the information on the detector sensitivity, both as functions of frequency and source sky position.

For a network of D detectors, equation (7) can be written in the equivalent matrix form

$$\begin{bmatrix} \tilde{d}_{w1} \\ \tilde{d}_{w2} \\ \vdots \\ \tilde{d}_{wD} \end{bmatrix} = \begin{bmatrix} F_{w1}^+ & F_{w1}^\times \\ F_{w2}^+ & F_{w2}^\times \\ \vdots & \vdots \\ F_{wD}^+ & F_{wD}^\times \end{bmatrix} \begin{bmatrix} \tilde{h}_+ \\ \tilde{h}_\times \end{bmatrix} + \begin{bmatrix} \tilde{n}_{w1} \\ \tilde{n}_{w2} \\ \vdots \\ \tilde{n}_{wD} \end{bmatrix}, \quad (9)$$

or

$$\tilde{\mathbf{d}}_w = \mathbf{F}_w \tilde{\mathbf{h}} + \tilde{\mathbf{n}}_w, \quad (10)$$

where we use boldface to denote vectors and matrices. Here

$$\tilde{\mathbf{h}} \equiv \begin{bmatrix} \tilde{h}_+ \\ \tilde{h}_\times \end{bmatrix}, \quad (11)$$

and the matrix \mathbf{F}_w is defined as

$$\mathbf{F}_w(\hat{\Omega}_s, f) \equiv \begin{bmatrix} \mathbf{F}_w^+ & \mathbf{F}_w^\times \end{bmatrix} = \begin{bmatrix} F_{w1}^+ & F_{w1}^\times \\ F_{w2}^+ & F_{w2}^\times \\ \vdots & \vdots \\ F_{wD}^+ & F_{wD}^\times \end{bmatrix}. \quad (12)$$

D	Number of detectors in the network.
$\alpha, \beta \in [1, \dots, D]$	Index specifying detector.
\mathbf{X}	(Boldface) A vector or matrix on the space of detectors.
\mathbf{X}^T	Matrix transpose of \mathbf{X} .
N	Number of data samples from each detector being analyzed.
$j, k \in [0, \dots, N - 1]$	Index specifying time or frequency sample.
h_+, h_\times	“Plus” and “cross” polarization waveforms of the gravitational wave.
$\hat{\Omega}_s$	Sky position of the gravitational-wave source.
$\hat{\Omega}$	Trial sky position.
$\mathbf{d}, \mathbf{n}, \mathbf{F}$	Data, noise, and antenna responses in strain.
$\mathbf{d}_w, \mathbf{n}_w, \mathbf{F}_w$	Noise-weighted (whitened) data, noise, and antenna responses.

TABLE I: Notation conventions for commonly used quantities in this paper.

This form makes it clear that, regardless of the functional form of $\tilde{h}_{+, \times}$, the gravitational-wave burst can only contribute to the network output along the directions \mathbf{F}_w^+ and \mathbf{F}_w^\times . The construction of null streams is thus obvious: we simply project the data $\tilde{\mathbf{d}}$ orthogonally to these directions. Formally, we select a new orthonormal Cartesian coordinate basis \mathbf{e}_i for the space of $\tilde{\mathbf{d}}$ in which vectors \mathbf{e}_{D-1} and \mathbf{e}_D span \mathbf{F}_w^+ and \mathbf{F}_w^\times . The remaining basis vectors $\mathbf{e}_1, \dots, \mathbf{e}_{D-2}$ are then orthogonal to \mathbf{F}_w^+ and \mathbf{F}_w^\times ,

$$\mathbf{F}_w^+ \cdot \mathbf{e}_i = 0 = \mathbf{F}_w^\times \cdot \mathbf{e}_i \quad i \in \{1, \dots, D - 2\}. \quad (13)$$

We say that the $\mathbf{e}_{i=1, \dots, D-2}$ form an orthonormal basis for the *null space* of \mathbf{F}_w^T [33], hence the term “null stream formalism.” We then construct a $(D - 2) \times D$ matrix \mathbf{A} whose rows are the components of this orthonormal basis,

$$\mathbf{A}(\hat{\Omega}_s, f) \equiv \begin{bmatrix} \mathbf{e}_1^T \\ \vdots \\ \mathbf{e}_{D-2}^T \end{bmatrix}. \quad (14)$$

By construction \mathbf{A} is orthogonal to \mathbf{F}_w^+ and \mathbf{F}_w^\times , so

$$\mathbf{A} \mathbf{F}_w = 0. \quad (15)$$

We obtain the null streams $\tilde{\mathbf{z}}$ by applying \mathbf{A} to the network data vector:

$$\begin{aligned} \tilde{\mathbf{z}} &\equiv \mathbf{A} \tilde{\mathbf{d}}_w \\ &= \mathbf{A} \mathbf{F}_w \tilde{\mathbf{h}} + \mathbf{A} \tilde{\mathbf{n}}_w \\ &= \mathbf{A} \tilde{\mathbf{n}}_w. \end{aligned} \quad (16)$$

The two independent strain components $\tilde{h}_{+, \times}$ are canceled out as a consequence of the definition (15) of the null space, making each \tilde{z}_α a *null stream*.

For example, the three-detector case is particularly simple. In this case the matrix \mathbf{A} is equal to

$$\mathbf{A} = \frac{\mathbf{F}_w^+ \times \mathbf{F}_w^\times}{|\mathbf{F}_w^+ \times \mathbf{F}_w^\times|}. \quad (17)$$

This is illustrated schematically in Figure 2. In the general case \mathbf{A} can be obtained either via singular value decomposition [17] or by explicitly constructing the associated projection operator (see Appendix A for details).

Note that \mathbf{A} is a function of the sky position (through $\mathbf{F}_w^{\times, \times}(\hat{\Omega}_s)$) and frequency (through $S_\alpha(f)$). The GWB will only be canceled when \mathbf{A} is evaluated for the correct source location, since generally

$$\mathbf{A}(\hat{\Omega}, f) \mathbf{F}_w(\hat{\Omega}', f) \neq 0. \quad (18)$$

In the next subsection we will discuss how to deal with the case where the source location is not known.

In the preceding discussion we have assumed implicitly that \mathbf{F}_w^+ and \mathbf{F}_w^\times are independent. In the general case the number of independent null streams is $D - r$, where r is the number of independent columns of \mathbf{F} , i.e.

$$r \equiv \text{rank}(\mathbf{F}_w). \quad (19)$$

There are two cases

1. If at least one detector in the network has a different alignment from the others then \mathbf{F}_w^+ and \mathbf{F}_w^\times are independent and $\text{rank}(\mathbf{F}_w) = 2$. In this case there are $D - 2$ null streams, and the method is applicable to networks of $D \geq 3$ detectors.
2. If all detectors in the network are aligned then $\mathbf{F}_w^+ \propto \mathbf{F}_w^\times$ and $\text{rank}(\mathbf{F}_w) = 1$. In this case there are $D - 1$ null streams, and the method is applicable to networks of $D \geq 2$ detectors.

Although in this paper we will concentrate on case 1, i.e. three or more non-aligned interferometers, we emphasize that our method works also with aligned detectors.

C. Null-stream analysis

Since the \mathbf{e}_i are orthonormal by construction, it follows that

$$\mathbf{A} \mathbf{A}^T = \mathbf{I}_{(D-2) \times (D-2)}. \quad (20)$$

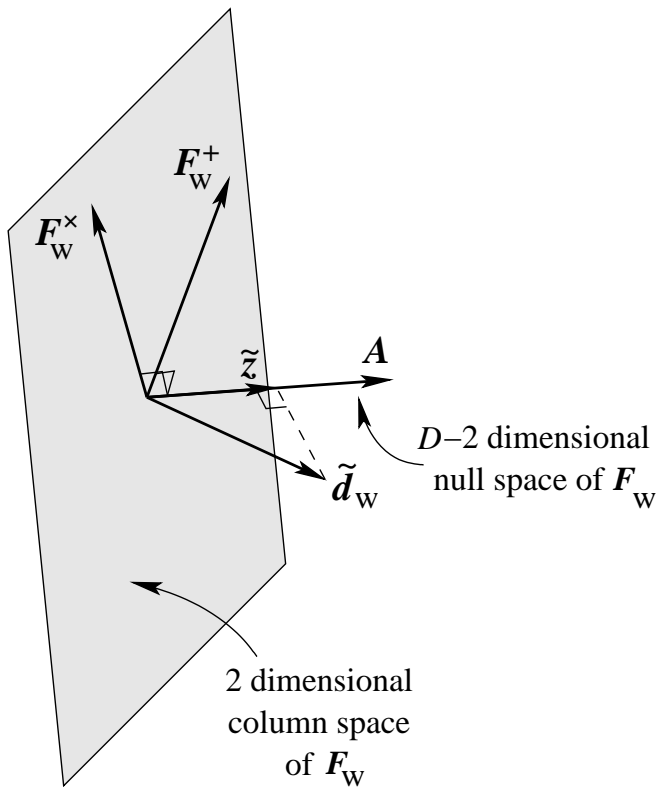


FIG. 2: Geometry of the null stream construction for the 3-detector case. The null stream is obtained by projecting the data along the vector \mathbf{A} , which is orthogonal to \mathbf{F}_W^+ and \mathbf{F}_W^x . For D non-aligned detectors \mathbf{A} has $D - 2$ dimensions.

This implies that each \tilde{z}_α is a Gaussian random process of unity variance and is uncorrelated with \tilde{z}_β , for all $\beta \neq \alpha$. This is the main advantage of the null-stream formalism over other techniques: *the noise distribution of the projected network data is known a priori, regardless of the form of $h_{+, \times}$, under the assumption that a GWB from a particular direction is present.* This allows us to perform statistically significant tests of the network data, in particular to test the hypothesis that a GWB from a given direction is present.

Since data from gravitational-wave detectors are sampled and digitized, in what follows we will consistently use discrete notation in our analysis of the statistics of the null stream. Our conventions for discretely sampled data are as follows: the Fourier-transform pair becomes

$$\begin{aligned} \tilde{x}[k] &= \sum_{j=0}^{N-1} x[j] e^{-i2\pi jk/N}, \\ x[j] &= \frac{1}{N} \sum_{k=0}^{N-1} \tilde{x}[k] e^{i2\pi jk/N}, \end{aligned} \quad (21)$$

where N is the number of data points in the time domain. Denoting the sampling rate by f_s , we can convert from continuous to discrete notation using $x(t) \rightarrow x[j]$, $\tilde{x}(f) \rightarrow f_s^{-1} \tilde{x}[k]$, $\int dt \rightarrow f_s^{-1} \sum_j$, $\int df \rightarrow f_s N^{-1} \sum_k$, $\delta(t - t') \rightarrow$

$f_s \delta_{jj'}$, and $\delta(f - f') \rightarrow N f_s^{-1} \delta_{kk'}$. For example, the one-sided strain noise power spectrum $S_\alpha[k]$ is

$$\langle \tilde{n}_\alpha^*[k] \tilde{n}_\beta[k'] \rangle = \frac{N}{2} \delta_{\alpha\beta} \delta_{kk'} S_\alpha[k]. \quad (22)$$

We will whiten the data by applying a zero-phase whitening filter [18, 19], and our normalization convention for whitened data is

$$\langle \tilde{n}_{w\alpha}^*[k] \tilde{n}_{w\beta}[k'] \rangle = \delta_{\alpha\beta} \delta_{kk'}. \quad (23)$$

The total energy in the null streams is

$$E_{\text{null}} \equiv \sum_{\alpha=1}^{D-r} \sum_{k=0}^{N-1} |\tilde{z}_\alpha[k]|^2. \quad (24)$$

Using (20) and (23) it follows that at the true source position $2E_{\text{null}}$ is χ^2 -distributed with $2N(D - r)$ degrees of freedom. In this case the expectation value of the null energy and its variance are both $N(D - r)$.

Although our considerations so far have assumed the sky position $\hat{\Omega}_s$ of the GWB source to be known *a priori*, in practice this may not be the case. Since we know that at the correct source location the null energy will not contain any contribution from the signal, a straightforward procedure is to scan over a grid of sky positions in search of the minimum of the null energy. Gürsel and Tinto [13] used time-delay estimates to limit their search to two possible regions of the sky (the regions around points S and S' in Figure 1). This approach may fail when the duration of the signals (or the timing uncertainty) is of the same order as the light travel time between detectors, thus necessitating an all-sky search. Since the numerical analysis in [13] implies that the characteristic angular width of the minimum of the null energy in a neighborhood of the source location for a GWB with a central frequency of about 100 Hz is equal to approximately 10^{-2} steradian for high SNRs, it follows that an all-sky search should be performed over a sky grid containing more than 10^3 resolvable directions. (Our numerical tests use a grid containing 10^4 points.) In either case, for each trial direction one postulates the presence of a gravitational-wave signal, forms a linear combination of the detectors that is orthogonal to that postulated direction, and χ^2 -tests this null stream for excess energy. If there exists a particular direction for which there is no excess energy in the null stream, the data is regarded as consistent with the hypothesis that a gravitational-wave burst is present and incoming from the inferred direction. If, on the other hand, E_{null} is inconsistent with a χ^2 distribution, then one rejects the hypothesis that a GWB is present incoming from that direction. The best estimate of the source direction is taken as the direction with minimum χ^2 .

Although the null-stream method does not require knowledge of the two GWB waveforms for its implementation, once the source location $\hat{\Omega}_s$ has been identified it is straightforward to reconstruct $h_{+, \times}$ from the data themselves [13] (if the detectors are all aligned then

only one of the polarizations can be reconstructed.) The minimum-variance estimate of the two waveforms for a network containing an arbitrary number of non-aligned detectors is given in Appendix B.

The null-stream combination of the data from a three-detector network and the resulting χ^2 test were first derived (in a different way) by Gürsel and Tinto [13] for detectors whose noises are white. They also implemented a near-optimal filtering procedure to account for colored noise. Our approach builds on this by generalizing and simplifying the derivation of the null stream and waveform reconstruction to networks containing an arbitrary number of detectors with different colored noises. One can also show that the null-stream procedure is formally equivalent to the maximum-likelihood analyses presented in [6, 20], though we leave the demonstration to a future paper.

D. Distinguishing GWBs from Noise Transients

The numerical analysis performed by Gürsel and Tinto in [13] was not aimed at checking whether the null energy estimator could distinguish GWBs from noise-induced glitches. In fact, an analysis based purely on the null stream runs into difficulty when applied to data containing noise transients. Strong uncorrelated glitches generally will not cancel in the null stream combination because they are not correlated in amplitude and phase in a way consistent with a GWB, implying a $\chi^2 > 1$ per degree of freedom. However, a null-stream analysis of a real GWB may also produce $\chi^2 > 1$ per degree of freedom, due to imperfect cancellation of the GWB in the null stream. This may happen for various reasons, such as the use of a discrete sky grid, inaccurate calibration of the data, or imperfect whitening of non-stationary data. Thus, an analysis based purely on the null stream would be forced to either reject both glitches and GWBs or accept both. Further, counter to one's intuition, this problem could get *worse* with stronger signals.

Glitches can also fool a null-stream analysis in 3-detector networks when the transient is weak in at least one detector. This is because the non-observation of a signal by one detector α is *always* consistent with a GWB incident from a direction and polarization to which the detector responses $F_{w\alpha}^+$ and $F_{w\alpha}^\times$ are sufficiently small. For sky positions with $F_{w\alpha}^+ \sim F_{w\alpha}^\times \sim 0$ the null stream projection matrix \mathbf{A} reduces to

$$\mathbf{A}_{\beta\gamma} \rightarrow \delta_{\alpha\beta}\delta_{\alpha\gamma}, \quad F_{w\alpha}^+, F_{w\alpha}^\times \rightarrow 0. \quad (25)$$

That is, the null stream for this sky position reduces to the detector in which there is no transient. This gives a χ^2 per degree of freedom of order unity regardless of whether the transient in the other two detectors is due to a GWB or noise. (Equivalently, when only two detectors observe a signal, it is always possible to find $h_{+,\times}$ that fit the output of these two detectors.) Thus double-coincident glitches will always pass a χ^2 test for certain

areas on the sky. And while networks containing four or more detectors will be less affected by this problem [21] because the size of the region of the sky producing two or more simultaneous, below-threshold responses is smaller than that for a single response, it will not be null.

In what follows we propose a simple way to make null-stream analyses robust against glitches by comparing the amount of energy in the null streams to that expected if the transients are uncorrelated. Let us consider how the null stream energy E_{null} depends on the individual detector data streams $d_{w\alpha}$. By defining the matrix

$$\mathbf{Q} \equiv \mathbf{A}^T \mathbf{A}, \quad (26)$$

we may write (24) in the convenient form

$$E_{\text{null}}(\hat{\Omega}) = \sum_{k=0}^{N-1} \sum_{\alpha=1}^D \sum_{\beta=1}^D \tilde{d}_{w\alpha}^*[k] Q_{\alpha\beta}[k, \hat{\Omega}] \tilde{d}_{w\beta}[k] \quad (27)$$

$$= \sum_{k=0}^{N-1} \left[\tilde{d}_{w1}^* \cdots \tilde{d}_{wD}^* \right] \begin{bmatrix} Q_{11} & Q_{12} & \cdots & Q_{1D} \\ Q_{21} & Q_{22} & & Q_{2D} \\ \vdots & & & \vdots \\ Q_{D1} & Q_{D2} & \cdots & Q_{DD} \end{bmatrix} \begin{bmatrix} \tilde{d}_{w1} \\ \tilde{d}_{w2} \\ \vdots \\ \tilde{d}_{wD} \end{bmatrix}. \quad (28)$$

Note that the null energy contains contributions from both cross-correlation ($\tilde{d}_{w\alpha}^* \tilde{d}_{w\beta}$) and auto-correlation ($\tilde{d}_{w\alpha}^* \tilde{d}_{w\alpha}$) terms. If the signals in the various detectors are independent (as one might expect for noise glitches), then the expectation value of the cross-correlation terms in (28) will be small compared to that of the auto-correlation terms. In this case the expectation value of E_{null} is just the sum of the diagonal terms in (28):

$$\text{mean}(E_{\text{null}}(\hat{\Omega})) \rightarrow \sum_{k=0}^{N-1} \sum_{\alpha=1}^D Q_{\alpha\alpha}[k, \hat{\Omega}] |\tilde{d}_{w\alpha}[k]|^2. \quad (29)$$

Here the mean is an ensemble average over noise instantiations. This observation motivates the use of a new energy measure, the *incoherent energy* E_{inc} , defined as the autocorrelation contribution to the null energy:

$$E_{\text{inc}}(\hat{\Omega}) \equiv \sum_{k=0}^{N-1} \sum_{\alpha=1}^D Q_{\alpha\alpha}[k, \hat{\Omega}] |\tilde{d}_{w\alpha}[k]|^2. \quad (30)$$

If the transient signals in the various detectors are not correlated, then we expect the following approximate equality to hold:

$$\text{mean}(E_{\text{null}}) \simeq \text{mean}(E_{\text{inc}}). \quad (31)$$

If instead the signals in the detectors are correlated, as will be the case when a GWB is present in the data, then at the correct sky location the GWB contributions cancel in the null energy, and the following inequality should hold:

$$\text{mean}(E_{\text{null}}) < \text{mean}(E_{\text{inc}}). \quad (32)$$

Thus, a distinguishing feature of a GWB is that a significant fraction of the energy in the individual detector data streams is canceled in the null stream.

In our simulations we test two simple measures of the degree to which E_{null} and E_{inc} show the behavior expected of a GWB. These are the quantities $E_{\text{null}} - E_{\text{inc}}$ and $(E_{\text{null}} - E_{\text{inc}})/E_{\text{inc}} = E_{\text{null}}/E_{\text{inc}} - 1$, which represent respectively the amount of ‘‘correlated energy’’ and the ratio of ‘‘correlated energy’’ to ‘‘uncorrelated energy’’ in the data.

An example is shown in Figure 3. This figure shows the incoherent energy versus null energy for a GWB and a glitch of the same amplitude, evaluated for approximately 10^4 uniformly distributed sky locations (see III for details). We note that for both the GWB and the glitch there are sky positions for which the null energy is approximately unity, so that projection onto the null energy alone does not distinguish this glitch and GWB. However, glitches and GWBs scatter differently in terms of the two energy measures E_{null} and E_{inc} . This suggests a modified procedure for distinguishing GWBs from glitches: scan over the sky and look for directions for which E_{null} is significantly smaller than E_{inc} . If there exists a sky direction for which E_{null} is sufficiently small compared to E_{inc} , we conclude that the transient could indeed be a GWB. If instead there is no direction for which E_{null} is sufficiently small compared to E_{inc} , we conclude that the transient is not a GWB.

Strong GWBs that are not precisely canceled in the null stream (due to calibration errors, for example) and have $E_{\text{null}} > N(D - r)$ will still pass this test because $E_{\text{null}} < E_{\text{inc}}$. Double-coincident glitches will fail even though $E_{\text{null}} \simeq N(D - r)$ because they have $E_{\text{null}} \simeq E_{\text{inc}}$. Put another way, the incoherent energy provides a natural cutoff in the significance of a χ^2 per degree of freedom measurement. Intuitively, if the null stream cancels out some large fraction of the excess incoherent energy, then we expect the event to be a gravitational wave, even if $\chi^2 > 1$ per degree of freedom. The failure to cancel a significant portion of the incoherent energy will eliminate glitches even if $\chi^2 \simeq 1$ per degree of freedom.

To get more insight into the behavior and usefulness of these energy measures, let us consider in more detail their expectation values over noise instantiations. Allowing for the case in which the transient is not a GWB, we write

$$\tilde{d}_{w\alpha}[k] = \tilde{n}_{w\alpha}[k] + \tilde{g}_{w\alpha}[k], \quad (33)$$

where $g_{w\alpha}$ denotes the noise-weighted transient as seen in detector α . For example, if the transient is a GWB from the direction $\hat{\Omega}_s$, and the tested sky position is $\hat{\Omega}$, then

$$\begin{aligned} \tilde{g}_{w\alpha}[k] &= \frac{F_{\alpha}^{+}[k, \hat{\Omega}_s] \tilde{h}_{+}[k] + F_{\alpha}^{\times}[k, \hat{\Omega}_s] \tilde{h}_{\times}[k]}{\sqrt{\frac{N}{2} S_{\alpha}[k]}} \\ &\times e^{i2\pi f_s k / N (\Delta t_{\alpha}(\hat{\Omega}) - \Delta t_{\alpha}(\hat{\Omega}_s))}. \end{aligned} \quad (34)$$

The phase term accounts for time shifting based on the

incorrect sky location $\hat{\Omega}$ instead of the true but unknown sky location $\hat{\Omega}_s$.

For simplicity, let us restrict ourselves to the case of detectors with equal noise spectra, for which \mathbf{Q} is independent of frequency. Then the noise-weighted transient signal $g_{w\alpha}$ appears in the null and incoherent energies in the combination

$$\rho_{\alpha\beta}^2 \equiv \sum_{k=0}^{N-1} \tilde{g}_{w\alpha}^*[k] \tilde{g}_{w\beta}[k] = \sum_{k=0}^{N-1} \frac{\tilde{g}_{\alpha}^*[k] \tilde{g}_{\beta}[k]}{\frac{N}{2} \sqrt{S_{\alpha}[k] S_{\beta}[k]}}, \quad (35)$$

which is the noise-weighted cross-correlation of the signals in detectors α and β . The diagonal terms are

$$\begin{aligned} \rho_{\alpha\alpha}^2 &\equiv \sum_{k=0}^{N-1} |\tilde{g}_{w\alpha}[k]|^2 = \sum_{k=0}^{N-1} \frac{|\tilde{g}_{\alpha}[k]|^2}{\frac{N}{2} S_{\alpha}[k]} \\ &\leftrightarrow 2 \int_{-\infty}^{\infty} df \frac{|\tilde{g}_{\alpha}(f)|^2}{S_{\alpha}(f)}. \end{aligned} \quad (36)$$

This autocorrelation term is simply the squared signal-to-noise ratio of an optimal matched filter for the transient in detector α , as indicated by the second line of (36).

As an example, let us consider the special case of a linearly polarized GWB (e.g., with $h_{\times} = 0$), with trial sky position $\hat{\Omega}$ and true source position $\hat{\Omega}_s$. In this case the cross-SNR is equal to

$$\begin{aligned} \rho_{\alpha\beta}^2 &\longrightarrow \frac{2}{N} \sum_{k=0}^{N-1} F_{\alpha}^{+}[k, \hat{\Omega}_s] F_{\beta}^{+}[k, \hat{\Omega}_s] \times \\ &\times \frac{|\tilde{h}_{+}[k]|^2}{\sqrt{S_{\alpha}[k] S_{\beta}[k]}} \cos \Psi_{\alpha\beta}(\hat{\Omega}, \hat{\Omega}_s) \end{aligned} \quad (37)$$

(only the real part of $\rho_{\alpha\beta}^2$ contributes to the energies), where the phase error is

$$\begin{aligned} \Psi_{\alpha\beta}(\hat{\Omega}, \hat{\Omega}_s) &= 2\pi \frac{f_s k}{N} (\Delta t_{\alpha}(\hat{\Omega}) - \Delta t_{\alpha}(\hat{\Omega}_s) \\ &- \Delta t_{\beta}(\hat{\Omega}) + \Delta t_{\beta}(\hat{\Omega}_s)). \end{aligned} \quad (38)$$

The cross-SNR $\rho_{\alpha\beta}^2$ for $\alpha \neq \beta$ is typically of the same order of magnitude as $\rho_{\alpha\alpha}^2$, but it is positive or negative depending on the timing error between pairs of detectors. As we test different positions on the sky, the timing errors change and the GWB contributions from the different detectors move in and out of phase. This will produce interference fringes in maps of E_{null} , $E_{\text{null}} - E_{\text{inc}}$, and $E_{\text{null}}/E_{\text{inc}}$. The location and spacing of these fringes are determined by the dominant frequency of the signal, the true sky position of the source, and the detector geometries and relative locations.

In terms of the SNRs (35), (36), the expectation values of the lowest moments of E_{null} , E_{inc} , and $E_{\text{null}} - E_{\text{inc}}$ are

$$\text{mean}(E_{\text{null}}) = N(D - r) + \sum_{\alpha=1}^D \sum_{\beta=1}^D Q_{\alpha\beta} \rho_{\alpha\beta}^2, \quad (39)$$

$$\text{var}(E_{\text{null}}) = N(D - r) + 2 \sum_{\alpha=1}^D \sum_{\beta=1}^D Q_{\alpha\beta} \rho_{\alpha\beta}^2, \quad (40)$$

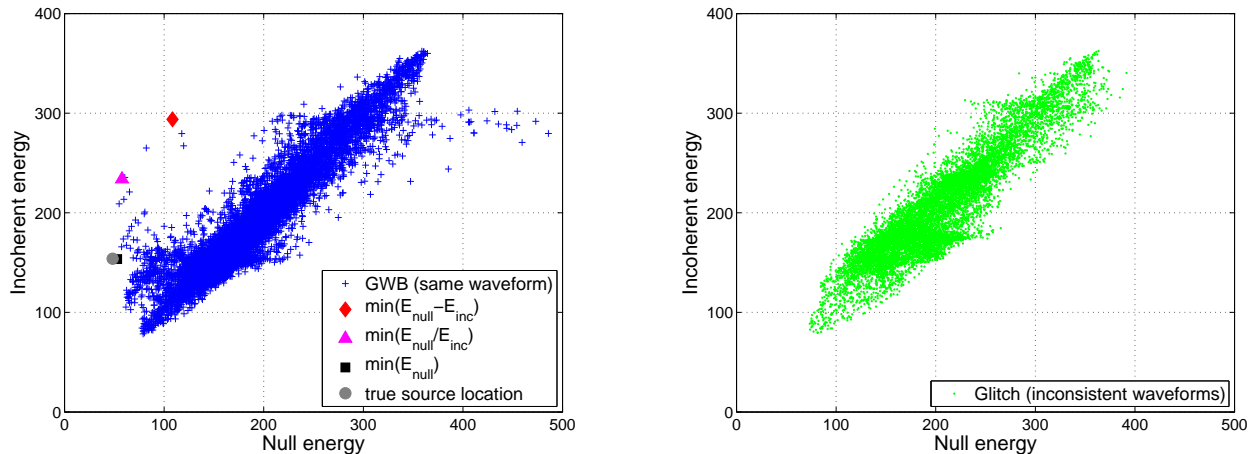


FIG. 3: Scatter plot of the null and incoherent energies for a simulated GWB (left) and a simulated glitch (right) seen in a network consisting of the LIGO-Hanford and LIGO-Livingston 4 km detectors and Virgo. In both cases the signal was scaled to rms SNR of 20 over the three detectors. Each point represents one trial sky position; approximately 10^4 sky positions in a uniform grid were tested. The waveforms and detector network used are discussed in detail in Section III. The GWB and glitch signals have the same signal-to-noise ratios and time delays in the individual detectors, and so are indistinguishable to incoherent tests. Note that for both the GWB and the glitch there are sky positions for which the null energy is consistent with noise ($E_{\text{null}} \simeq N(D-r) = 60$ for these simulations). However, for the GWB there are also sky positions with $E_{\text{null}} \ll E_{\text{inc}}$ (points above the diagonal); these are due to the fact that the GWB signal is correlated between the detectors. The glitch signal does not access this portion of the $(E_{\text{null}}, E_{\text{inc}})$ space. This observation is the basis of our consistency test; we scan over the sky and look for directions where $E_{\text{null}} < E_{\text{inc}}$. The true source location is indicated by the circle on the GWB plot. Also shown on the GWB plot are the tested sky positions which have the smallest values of $E_{\text{null}} - E_{\text{inc}}$, $E_{\text{null}}/E_{\text{inc}}$, and E_{null} . The sky maps for these same simulations are shown in Figure 4.

$$\text{mean}(E_{\text{inc}}) = N(D-r) + \sum_{\alpha=1}^D Q_{\alpha\alpha} \rho_{\alpha\alpha}^2, \quad (41)$$

$$\text{var}(E_{\text{inc}}) = N \sum_{\alpha=1}^D Q_{\alpha\alpha}^2 + 2 \sum_{\alpha=1}^D Q_{\alpha\alpha}^2 \rho_{\alpha\alpha}^2, \quad (42)$$

$$\text{mean}(E_{\text{null}} - E_{\text{inc}}) = \sum_{\alpha=1}^D \sum_{\beta=1}^D (1 - \delta_{\alpha\beta}) Q_{\alpha\beta} \rho_{\alpha\beta}^2, \quad (43)$$

$$\begin{aligned} \text{var}(E_{\text{null}} - E_{\text{inc}}) &= N \sum_{\alpha=1}^D \sum_{\beta=1}^D (1 - \delta_{\alpha\beta}) Q_{\alpha\beta}^2 + \\ &+ 2 \sum_{\alpha=1}^D \sum_{\beta=1}^D \sum_{\gamma=1}^D (1 - \delta_{\alpha\beta})(1 - \delta_{\alpha\gamma}) Q_{\alpha\beta} Q_{\alpha\gamma} \rho_{\alpha\gamma}^2. \end{aligned} \quad (44)$$

We note that the signal enters E_{inc} only through its SNR $\rho_{\alpha\alpha}^2$ in the individual detectors; E_{inc} does not depend on the structure of the transient signal. As a result, variations in E_{inc} reflect variations in the network sensitivity due to noise-weighted geometrical factors (the \mathbf{Q}) and do not contain significant information on the signal. By contrast, $E_{\text{null}} - E_{\text{inc}}$ contains only cross terms, and shows the interference of the signals measured by the different detectors.

For example, Figure 4 shows sky maps of the E_{null} , E_{inc} , and $E_{\text{null}}/E_{\text{inc}}$ [note that $E_{\text{null}}/E_{\text{inc}} = (E_{\text{null}} -$

$E_{\text{inc}})/E_{\text{inc}} + 1]$ for the same GWB and glitch signals used in Figure 3. The null energy maps for the GWB and the glitch are very similar. The GWB and glitch are constructed to have the same relative time delays and SNRs in the various detectors. As a result, the incoherent energy maps are virtually identical for the GWB and the glitch. Removing this signal-independent structure from the null energy makes the signal-dependent structure in the sky maps clearer. In particular, the plot of $E_{\text{null}}/E_{\text{inc}}$ for the GWB shows sharp interference fringes orthogonal to the Hanford-Livingston and Livingston-Virgo baselines (the signal was strongest in Livingston and Virgo in this simulation). The sky location of the GWB signal lies on one of the two intersection points of these interference fringes, so they can be used to locate the source. Such sharp features are not present in the corresponding sky map for the glitch, since the glitch waveforms are not strongly correlated.

We note from (39)-(44) that fractional fluctuations in the energies scale as $N^{-1/2}$ for weak signals. Since the signal-dependent structure scales as $\rho_{\alpha\beta}^2$, the basic limit of purely local measurements of sky maps scales as $\rho_{\alpha\beta}^2/N^{1/2}$. This is the same scaling as in excess-power searches [22].

Also, we note that if we restrict our analysis to a frequency range $f = kf_s/N \in [f_{\text{min}}, f_{\text{max}}]$, then N in (39)-(44) becomes the number of frequency bins actually summed over, and ρ^2 (35), (36) is to be computed over

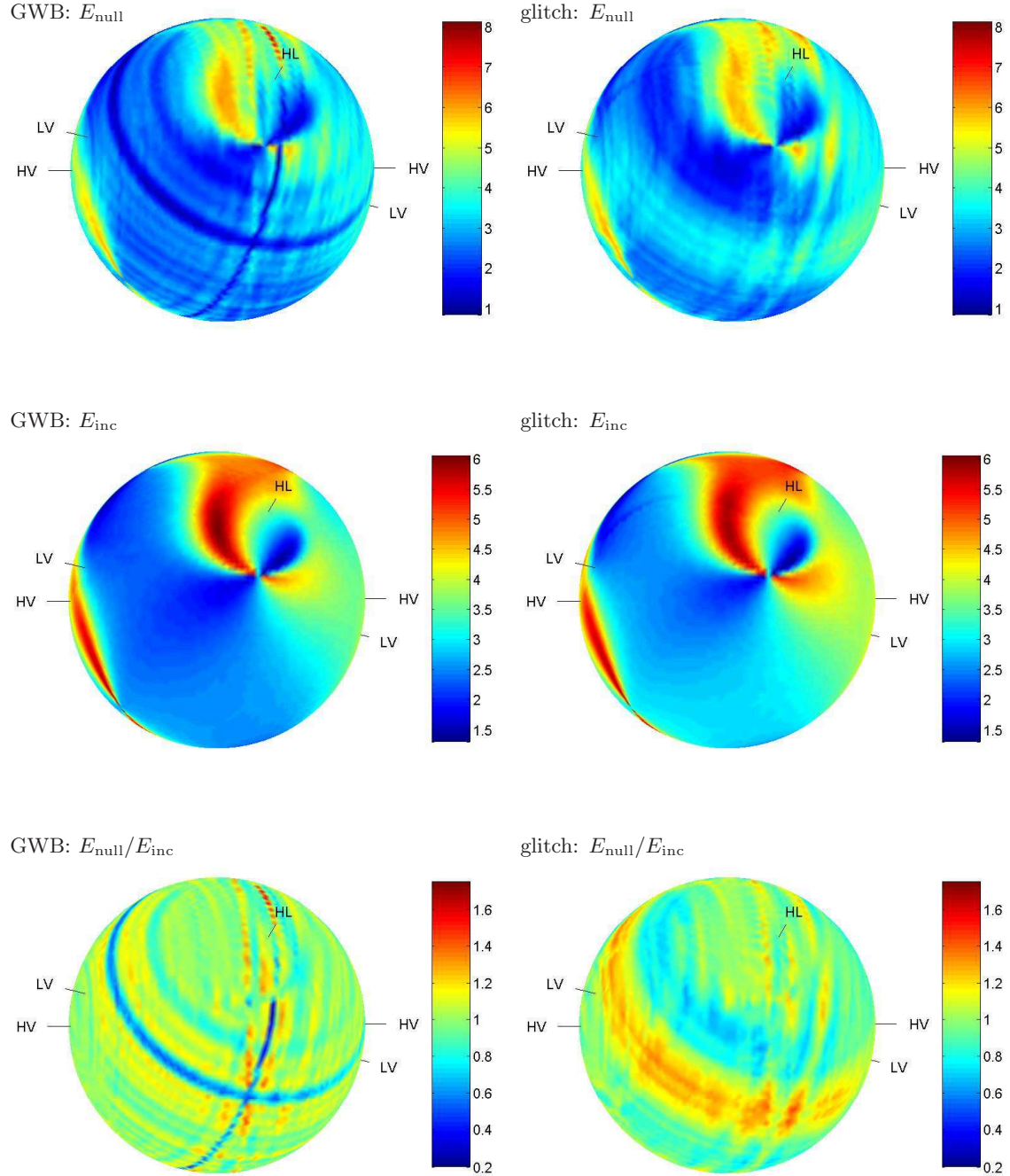


FIG. 4: Sample sky maps, normalized to $E/(N(D - r))$, for the same GWB and glitch signals used in Figure 3. The plots on the left are for a GWB with rms SNR of 20 in the three detectors. Those on the right are for a glitch with the same relative time delays and signal energies in each detector as the GWB. (Note that these two events are indistinguishable to an incoherent analysis.) The network consists of the LIGO-Hanford (H) and LIGO-Livingston (L) 4 km detectors and Virgo (V). The null energy map (top) shows interference fringes due to the transient signal, as well as structure due to the network geometry. They are very similar for the GWB and the glitch. The incoherent energy map (middle) is constructed from the auto-correlations of the individual detector data streams and reflects variations in the network sensitivity over the sky. It is virtually identical for the GWB and the glitch because the two events have the same relative time delays and SNRs. Dividing out the incoherent energy from the null energy (bottom) removes this structure associated with the network geometry, making the signal-dependent structure clearer. The GWB map shows sharp interference fringes (blue and red rings) where the time delays along the H-L, L-V, and H-V baselines match those of the source location. There is little of such structure in the glitch map.

the same (positive) frequency range.

Finally, we point out that in the high SNR limit the minimum of the null energy E_{null} occurs at the source location [13], which is useful for solving the inverse problem for bursts. The incoherent energy E_{inc} is *not* an extremum at the source location, so measures like $E_{\text{null}}/E_{\text{inc}}$ and $E_{\text{null}} - E_{\text{inc}}$ cannot directly resolve the source location. As noted above, however, the clearer signal-dependent structure in $E_{\text{null}} - E_{\text{inc}}$ and $E_{\text{null}}/E_{\text{inc}}$ compared to E_{null} may be useful for this purpose. In any case, our consistency test can improve the detection confidence of a gravitational-wave burst, and should be regarded as an essential first step in solving the inverse problem.

E. Sensitivity of the method to data calibration

The derivation of the null-stream combinations described in subsection IIB assumed the data from the interferometers to be perfectly calibrated. This means that properly modeled transfer functions of the interferometer responses (which depend on various parameters associated with the characteristics of the cavities of the interferometers) are applied to the raw data in order to obtain strain measurements. In practice, however, the parameters describing these transfer functions are known with finite accuracy, in turn preventing the null-stream combinations from exactly canceling the GWB signal at the correct source location. In order to quantify the effect on our method we should note that the magnitude of the residual signal in the null-stream combinations will be proportional to the accuracy by which the calibration parameters are known. For the LIGO detectors the calibration parameters are known to better than ten percent [23]. Preliminary studies indicate our consistency test is robust against calibration errors of this size; these effects will be studied in more detail in a future article.

F. Implementation

Our null-stream based analysis has been implemented as a publicly available MATLAB package, “XPIPELINE” [24]. For a specific detector network and event time, XPIPELINE reads the appropriate data from frame files [25] (the standard format for storing data from gravitational-wave detectors), optionally injects GWB signals and/or glitches, whitens the data, computes the null stream coefficient matrix \mathbf{A} for each specified sky direction and frequency, computes the time shifts for each direction, steps through data in overlapping blocks of user-specified duration, time shifts the data to the nearest sample, Fourier transforms it, completes the time shift with a phase rotation, forms the null stream in the frequency domain, sums the power in user-specified frequency bands, and records the null and incoherent energies for each time-frequency band and direction.

XPIPELINE runs in approximately 1/100th real time. For example, the analysis of the 10^4 simulated events used to produce Figures 6-11 took approximately 16 hours on 4 Intel Pentium 4, 2.66 GHz computers. This makes our null-stream-based consistency test feasible as a follow-up test in GWB searches.

III. SIMULATIONS

A. Network and signal types

To test the efficacy of our statistical test in discriminating GWBs from noise glitches in the $(E_{\text{null}}, E_{\text{inc}})$ space, we need to select a detector network, a population of GWBs, and a population of glitches.

We elect to simulate a network consisting of the Hanford and Livingston 4 km interferometers (“H” and “L”) and a third identical instrument at the Virgo site (“V”). For the sake of simplicity we neglect both the Hanford 2 km interferometer and the differences between the LIGO and Virgo design sensitivities. The locations \vec{r}_α and orientations (which determine F^+ , F^\times) of the interferometers are taken from [22, 26]. The calibrated stationary background noise $n_\alpha[j]$ for H and L are taken from a standard 24 hour reference simulation [27]. The background noise for V is taken from the Hanford simulation with a 2 second time shift, which is much larger than the time scales of the signals used in this analysis.

The next step is to select the GWB and glitch waveforms. To simulate a glitch, we need three waveforms (one for each detector) that are not strongly correlated. To simulate GWBs we wish to use waveforms that are motivated by astrophysical considerations. Our consistency test is ultimately based on the fact that for a GWB the signal seen in each detector is correlated in a particular way, whereas for a glitch the signals generally will not be correlated. In order to show that our test does not rely on any fundamental difference between “typical” GWB waveforms and “typical” glitch waveforms, we elect to use the *same* set of waveforms for simulating GWBs and glitches. We select three representative waveforms from the Dimmelmeier-Font-Mueller (“DFM”) catalog [9] of Type II core-collapse supernovae. Specifically, we choose the A1B3G3 “regular collapse” waveform, the A1B3G5 “rapid collapse” waveform, and the A3B4G2 “multiple bounce” waveform. Figure 5 shows the time-series and power spectra of these waveforms. As we shall see below, these three waveforms have moderately low but nonzero cross-correlations.

To simulate a gravitational-wave signal, one of the three waveforms is randomly selected and added into the data stream from each interferometer, with time delays and scaling appropriate for some choice of polarization angle and location on the sky. To simulate a glitch we follow the same procedure, except that a different waveform is selected for each detector. The scaling and time delays proceed as for a GWB. This population of glitches has

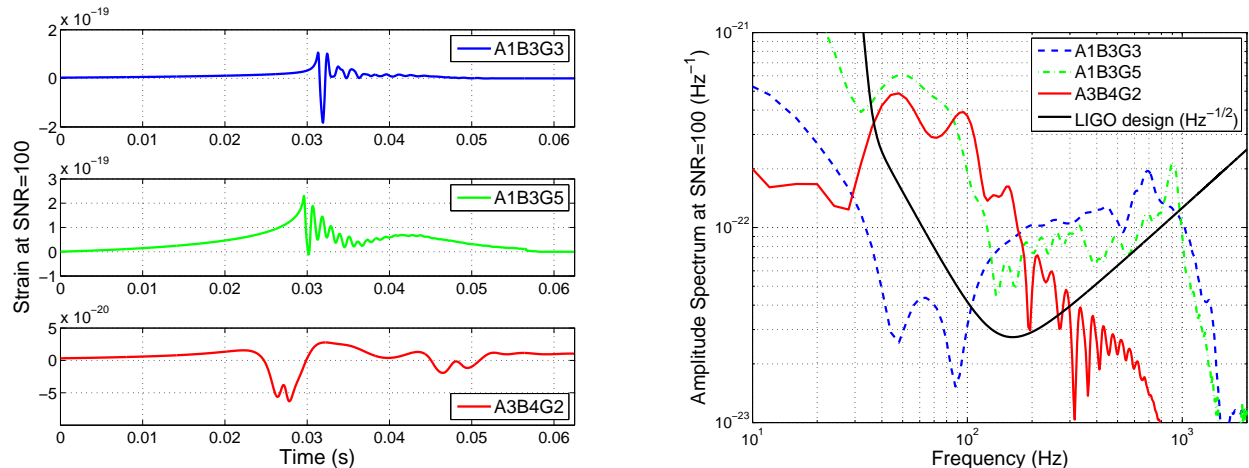


FIG. 5: Dimmelmeier - Font - Mueller (“DFM”) waveforms used to simulate GWBs and glitches in our analysis. Left plot: time series waveforms scaled to $\text{SNR} = 100$ for optimal orientation. (The linear trend present in the original waveforms has been removed.) Right plot: spectra with a 1 Hz resolution; shown for comparison is the LIGO design noise curve used for both LIGO and Virgo detectors.

the property that it would pass any incoherent test, as the arrival times, power distribution, and even frequency bands are consistent with those of true gravitational-wave signals. We stress that, though not a realistic glitch population, this provides us with examples of the kind of pathological glitches that cannot be dismissed by per-detector methods.

B. Analysis parameters

The main tunable parameters in our analysis are the time and frequency bands and the sky positions to test. Ideally the integration time and frequency band should be matched to the signal being tested, to maximize the signal-to-noise ratios $\rho_{\alpha\alpha}^2$ and minimize the background noise contribution $N(D - r)$. We choose an integration length of $1/16$ s, which is the smallest power of 2 larger than the durations of the three sample waveforms tested. We overlap consecutive data segments by 50% to minimize the loss of signal-to-noise when a signal overlaps the edge of a data segment. We use a single frequency band [34] of $[64, 1024]$ Hz. The upper frequency limit is set by the highest frequency at which our target signals have significant power compared to the noise curve; see Figure 5. The lower limit is set at 64 Hz because the actual noise level in current detectors is larger than the design noise below this cutoff [28].

Once the locations of the detectors and the upper bound on frequencies involved in the analysis are known, a set of directions $\{\hat{\Omega}\}$ covering the sky may be produced. Both the projection matrix \mathbf{Q} (26) and the time delays Δt_α (2) vary with angle, but the effect of Δt_α on the cross-correlation terms occurs on a smaller angular scale for most of the sky. A simple criteria then is to cover the

sky with a maximum angular mismatch defined by the longest detector baseline and the maximum frequency. As with all template placement problems we have some freedom in how to produce this set, and chose a somewhat sub-optimal but simple set of directions - a grid of approximately 10^4 points uniformly distributed in θ and $\phi \sin \theta$.

C. Waveform normalization

The DFM waveforms are linearly polarized, which means that the two polarizations are linearly dependent and so can be written in the form

$$h_+(t) = \cos(2\psi_s) h(t) \quad (45)$$

$$h_\times(t) = \sin(2\psi_s) h(t), \quad (46)$$

where ψ_s is the polarization angle. As a result, the strain signal g_α in detector α is

$$g_\alpha(t) = \left(F_\alpha^+(\hat{\Omega}_s) \cos 2\psi_s + F_\alpha^\times(\hat{\Omega}_s) \sin 2\psi_s \right) h(t). \quad (47)$$

These waveforms are de-trended and normalized against the interferometer noise curve so that $\rho_{\alpha\alpha}^2 = 1$ (36) for optimal orientation (the case $F_\alpha^+ \cos 2\psi_s + F_\alpha^\times \sin 2\psi_s = 1$, so that $g_\alpha(t) = h(t)$); i.e., we define the normalization of $h(t)$ so that

$$\sum_{k=0}^{N-1} \frac{|\tilde{h}[k]|^2}{\frac{N}{2} S[k]} = 1. \quad (48)$$

(Recall that our detectors have identical noise spectra, so $S_\alpha[k] = S_\beta[k] \equiv S[k]$.) The cross-correlations (35) of the waveforms depend on their relative time or phase shift;

with this normalization the maximum cross-correlations over all shifts for co-aligned detectors are

$$\max_{\Psi} \{\rho_{\alpha\beta}^2\} = \begin{cases} 0.58 & (\text{A1B3G3} - \text{A1B3G5}) \\ 0.26 & (\text{A1B3G3} - \text{A3B4G2}) \\ 0.50 & (\text{A1B3G5} - \text{A3B4G2}) \end{cases}. \quad (49)$$

For comparison, typical cross-correlation values for Gaussian noise in our time-frequency band are 0.15 – 0.2.

To simulate a gravitational wave signal, one of the three waveforms A1B3G3, A1B3G5, or A3B4G2 is randomly selected. Uniformly distributed random direction $\hat{\Omega}_s$ and polarization ψ_s angles are chosen. For each detector α , the discrete catalog waveform $h(t)$ is time-shifted by $\Delta t_\alpha(\hat{\Omega}_s)$ (2) and resampled to match $n_\alpha[j]$. The waveform is then scaled by the antenna response as in (47) to give g_α .

To characterize the efficacy of our consistency test as a function of the signal strength, we choose to simulate populations of candidates with the same *measured* signal-to-noise ratios; i.e., the signals are scaled so as to deliver a fixed total SNR to the network. This simulates candidates near a detection threshold, rather than (for example) a physical population of standard candles. With the normalization (48) and (47) one finds

$$\begin{aligned} \frac{1}{D} \sum_{\alpha=1}^D \rho_{\alpha\alpha}^2 &= \frac{1}{D} \sum_{\alpha=1}^D \sum_{k=0}^{N-1} \frac{|g_\alpha[k]|^2}{\frac{N}{2} S[k]} \\ &= \frac{1}{D} \sum_{\alpha=1}^D \left(F_\alpha^+(\hat{\Omega}_s) \cos 2\psi_s + F_\alpha^\times(\hat{\Omega}_s) \sin 2\psi_s \right)^2. \end{aligned} \quad (50)$$

To fix the SNR in the detectors to some rms value ρ_{rms} , we apply the further normalization

$$g_\alpha(t) \rightarrow \frac{g_\alpha(t) \rho_{\text{rms}}}{\sqrt{\frac{1}{D} \sum_{\beta=1}^D \left(F_\beta^+(\hat{\Omega}_s) \cos 2\psi_s + F_\beta^\times(\hat{\Omega}_s) \sin 2\psi_s \right)^2}}. \quad (51)$$

With this scaling we find

$$\sqrt{\frac{1}{D} \sum_{\alpha=1}^D \rho_{\alpha\alpha}^2} = \rho_{\text{rms}}. \quad (52)$$

To simulate a population of glitches, the same process was followed with the sole exception that a different DFM waveform was selected for each detector. We applied the same scaling and time delays as for a GWB. This population of glitches has the property that it would pass any incoherent test, as its arrival times and power distribution are consistent with those of true gravitational-wave signals. We reiterate that, though not a realistic glitch population, this provides us with examples of the kind of pathological glitches that cannot be dismissed by per-detector methods.

D. Analysis Procedure

After the signal has been added to the background noise, the data are whitened to produce $d_{\text{w}\alpha}[j]$. The whitening algorithm is trained on a 16 second block of data that does not include the signal. With a known set of trial sky positions $\{\hat{\Omega}\}$ and measured power spectra $S_\alpha(f)$, \mathbf{Q} can be computed for each direction and resolvable frequency.

For each direction on the sky, overlapping segments of data are considered sequentially, the length of the segments depending on the time scales of the signal under consideration (here chosen as 1/16 s). To perform the time shifts, the segments are extracted from the closest integer samples in the time domain, and then transformed to the Fourier domain where the remaining part of the time shift is performed by applying phase shifts. The null and incoherent energies are then computed and recorded for that direction on the sky.

For each simulation we select the two directions for which the transient shows the most correlation according to two different criteria, as well as the direction with the minimum null energy:

1. $\min(E_{\text{null}} - E_{\text{inc}})$: Measures the linear distance away from the diagonal in a scatter plot of E_{inc} vs. E_{null} (see Figure 3). Physically it represents the largest amount of energy canceled in forming the null stream.
2. $\min(E_{\text{null}}/E_{\text{inc}})$: Measures the angular distance away from the diagonal in a scatter plot of E_{inc} vs. E_{null} (see Figure 3). Physically it represents the largest fraction of energy canceled in forming the null stream.
3. $\min(E_{\text{null}})$: Calculated for comparison against the other two statistics, and for estimating the sky location.

Figures 6, 7, 8 show scatter plots of E_{inc} vs. E_{null} for the sky locations picked by these three criteria for 10^4 simulated signals. The signal population consists of 10^3 GWBs and 10^3 glitches at each of 5 different signal-to-noise ratios, $\rho_{\text{rms}} = 5, 10, 20, 50, 100$.

Note that there is a significant difference in the distributions of signals and glitches using any of the measures $\min(E_{\text{null}} - E_{\text{inc}})$, $\min(E_{\text{null}}/E_{\text{inc}})$, or $\min(E_{\text{null}})$. For both GWBs and glitches there are directions on the sky for which the null energy is low. However, for glitches these occur exclusively at low incoherent energies. For signals there exist directions with low null energy at larger incoherent energies. This restriction is strongest when measuring correlations using $\min(E_{\text{null}}/E_{\text{inc}})$ (Figure 6). For $\min(E_{\text{null}} - E_{\text{inc}})$ (Figure 7) there are a small but noticeable fraction of GWBs that overlap the glitch population and so are indistinguishable from glitches. By using instead $\min(E_{\text{null}})$ only (Figure 8) a significant fraction of the glitches have a sky location with low null energy, but only at low incoherent energy as well.

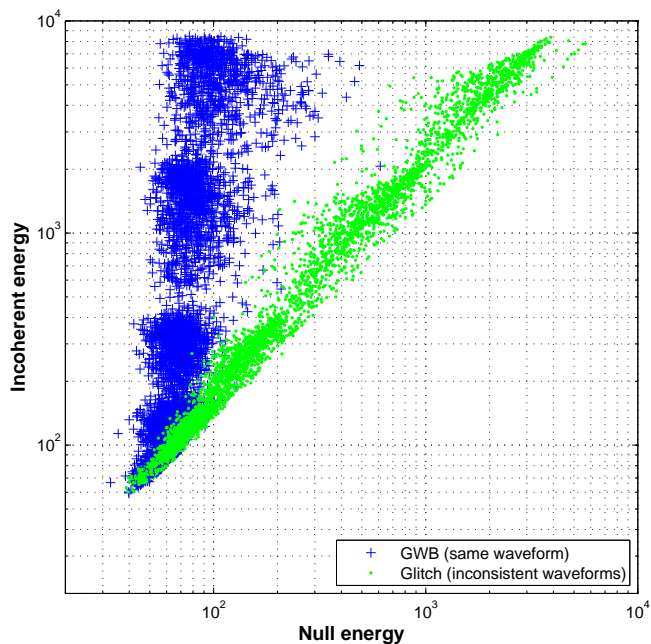


FIG. 6: Scatter plot of the null and incoherent energies for the most correlated direction on the sky, defined as the direction of $\min(E_{\text{null}}/E_{\text{inc}})$ (i.e., the upper left limit of Fig. 3), for glitches and GWBs of various signal-to-noise ratios. Note that as the signal-to-noise ratio increases (higher E_{inc}) the GWB and glitch distributions separate, with the GWBs remaining at relatively low null energies and the glitches having comparable null and incoherent energies. The clumping is due to the 5 distinct rms SNRs used in our simulations: 5, 10, 20, 50, 100. The null energies for some of the GWB simulations are greater than that expected (60) from the number of degrees of freedom because we are selecting sky positions from the minimum of $E_{\text{null}}/E_{\text{inc}}$, not from the minimum of E_{null} .

As the SNR increases the populations become distinct. We can see this in Figures 9-11, which show the Receiver-Operator Characteristic (ROC) curves for the performance of our various statistics in discriminating the two populations. At total energies corresponding to $\rho_{\text{rms}} \sim 10 - 20$ or greater we can detect most of a population of gravitational waves and reject essentially all of a population of semi-correlated glitches. The rejected gravitational waves are those that are weak in at least one detector, or equivalently produce little correlation.

For $\rho_{\text{rms}} = 5$ or lower the glitch and GWB populations are not distinct. This is because the null stream enforces waveform consistency only when there is excess energy to suppress.

IV. CONCLUSIONS AND FUTURE DIRECTIONS

In this article we have introduced an extension of the Gursel-Tinto null-stream technique that allows one to

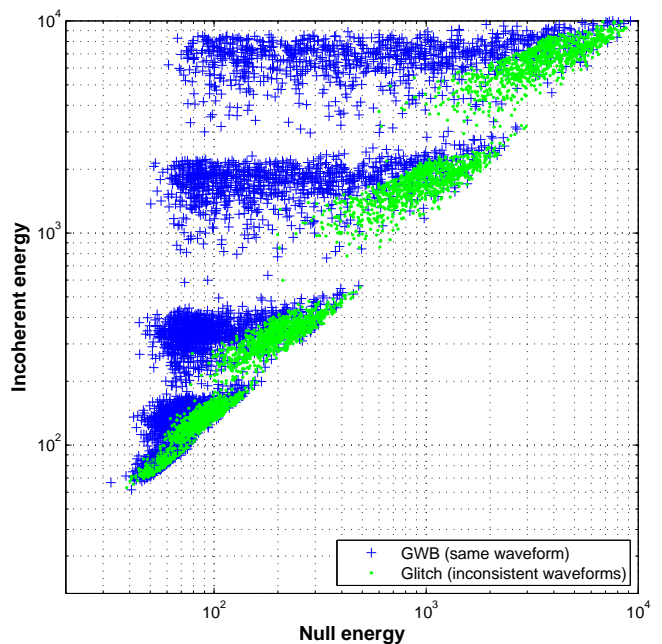


FIG. 7: Scatter plot of the null and incoherent energies for the most correlated direction on the sky, defined as the direction of $\max(E_{\text{inc}} - E_{\text{null}})$ (i.e., the upper left limit of Fig. 3), for glitches and GWBs of various signal-to-noise ratios. Note that as the signal-to-noise ratio increases (higher E_{inc}) the GWB and glitch distributions separate, with the GWBs remaining at relatively low null energies and the glitches having comparable null and incoherent energies. The clumping into horizontal bands is due to the 5 distinct rms SNRs used in our simulations: 5, 10, 20, 50, 100. The null energies for many of the GWB simulations are greater than that expected (60) from the number of degrees of freedom because we are selecting sky positions from the minimum of $E_{\text{null}} - E_{\text{inc}}$, not from the minimum of E_{null} .

make robust tests to distinguish between GWB signals and coincident noise glitches. This technique is based on comparing the energy in the null stream to that expected if the signals in the various detectors are uncorrelated, and does not require any *a priori* knowledge of the GWB or glitch waveforms. We applied this technique to the case of the LIGO-Virgo 3-detector network at design sensitivity, and quantified the ability of three different measures of correlation to distinguish true GWBs from coincident noise glitches. For the best-performing measure, the ratio of null energy to incoherent energy, we found that gravitational-wave bursts of SNR 10 – 20 or greater can be distinguished from glitches of comparable SNRs that are injected in the data with the same time delays but are different in the three detectors’ data. For example, with the GWB and glitch populations tested, we found that 90% of glitches can be rejected while accepting 94% of SNR 20 GWBs and 76% of SNR 10 GWBs. Furthermore, we stress that the glitch population tested was pathological in the sense that they were constructed to have time delays and amplitudes consistent with a GWB.

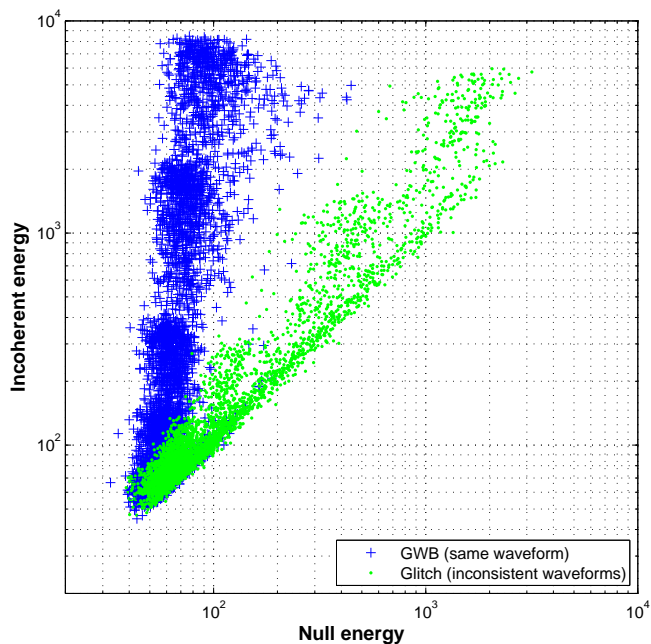


FIG. 8: Scatter plot of the null and incoherent energies for the best-fit direction on the sky, defined as the direction of $\min(E_{\text{null}})$ (i.e., the left-most point in Figure 3), for glitches and GWBs of various signal-to-noise ratios. Note that as the signal-to-noise ratio increases (higher E_{inc}) the GWB and glitch distributions separate, with the GWBs remaining at relatively low null energies and the glitches having comparable null and incoherent energies. The clumping is due to the 5 distinct rms SNRs used in our simulations: 5, 10, 20, 50, 100. Note that a large fraction of the glitch signals produce low null energies for some sky positions. This means that GWBs and glitches are not distinguishable using only the null energy.

Hence, the performance of the consistency test may be even better with real detector data. This consistency test is therefore a promising technique for rejecting noise coincidences and increasing detection confidence in GWB searches.

The development of coherent analysis techniques for GWB detection is still at an early stage, and much further research can be done. In this section we briefly outline some of the directions of current and future work. These can be divided roughly into applications of the existing consistency test to more general networks and signals, and extensions and improvements to the algorithm.

We will systematically study a larger variety of waveforms than the small set considered in the paper. These should include two-polarization GWBs. (The supernova waveforms used here are linearly polarized). This wider set may include various supernova catalogs [8, 9, 10], and approximate waveforms for black-hole binary coalescence (see for example [7]). The latter are particularly important, since it is quite plausible that black-hole binaries will be the first transient signals to be detected.

Another near-term goal is to apply our modified null-

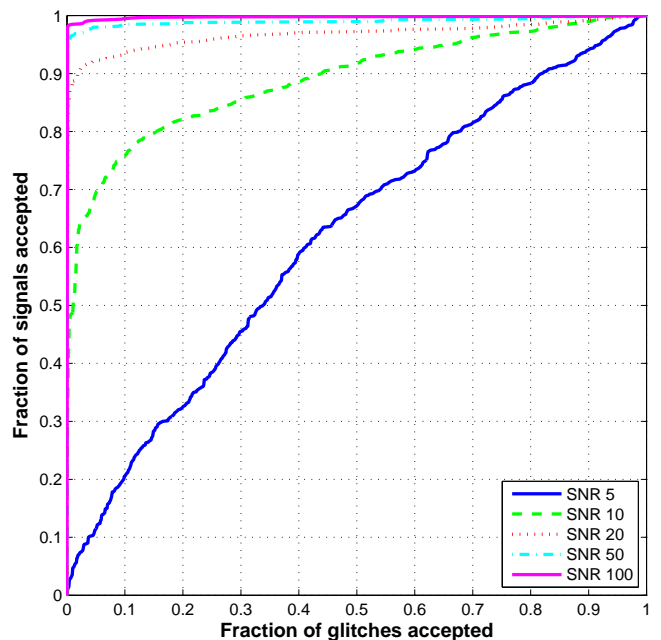


FIG. 9: Receiver-Operator Characteristic (ROC) plot for $\min(E_{\text{null}}/E_{\text{inc}})$ as a statistic for distinguishing GWBs from noise glitches. The ROC curve value is given by the fraction of GWBs (true acceptance) and glitches (false acceptance) of given rms SNR falling to the left of a line of constant $E_{\text{null}}/E_{\text{inc}}$ (a diagonal line) in Fig. 6. The rapid rise of the curves at low false acceptance is indicative of the ability of the method to confidently distinguish a significant portion of GWB signals from the glitch population.

stream test to other networks, such as those with four and five detectors. A fourth non-aligned detector will reduce the fraction of sky over which only two detectors have significant sensitivity [21], increasing the strength of the test. An additional aligned detector, such as the two-kilometer detector at LIGO-Hanford, would also provide a second null stream without extra sky coverage. Lazarini *et al.* [29] have demonstrated how the output of the two LIGO-Hanford detectors can be combined to form a single pseudo-detector with greater sensitivity than either. The difference between the detector outputs is also a null stream, effectively a detector with zero antenna response, which can be employed in our consistency test. This is a computationally cheap test since the H1-H2 null stream is independent of the sky position, providing the basis of a simple hierarchical analysis scheme.

We also plan to test the power of our consistency test on real data, with real noise transients. We should note that the artificial noise coincidences studied in this work are pathological in the sense that they are injected with time delays and amplitude responses consistent with actual sky positions, and waveforms that are identical (in individual detectors) to GWBs. Although we would not expect noise in actual detectors to be so pathological, it is important to characterize the robustness of our technique for real data, and this was the motivation for our

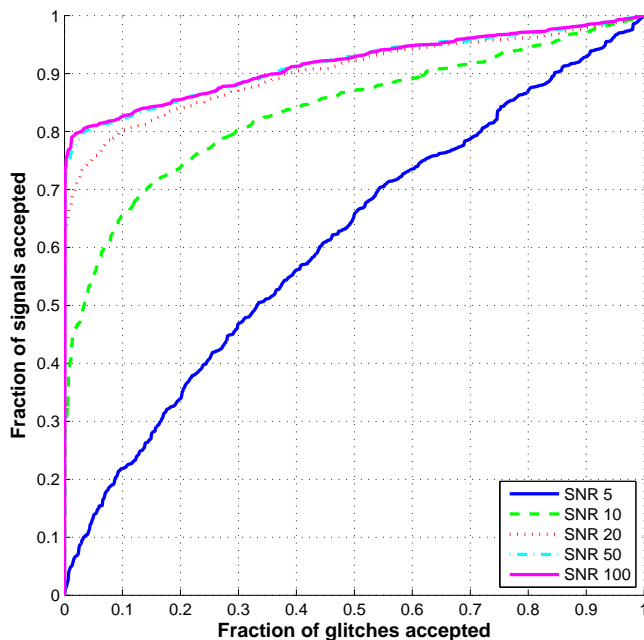


FIG. 10: Receiver-Operator Characteristic plot (ROC) for $\min(E_{\text{null}} - E_{\text{inc}})$ as a statistic for distinguishing GWBs from noise glitches. The ROC curve value is given by the fraction of GWBs (true acceptance) and glitches (false acceptance) of given rms SNR falling to the left of a line of constant $E_{\text{null}} - E_{\text{inc}}$ in Fig. 7. The rapid rise of the curves at low false acceptance is indicative of the ability of the method to confidently distinguish a significant portion of GWB signals from the glitch population. This is not as powerful a statistic as $\min(E_{\text{null}}/E_{\text{inc}})$ (see Figure 9).

implementation.

Another important aspect of real data is that their calibration could be inaccurate, implying an imperfect cancellation of the GWB by the null stream. We will study quantitatively the effects of realistic calibration errors on the effectiveness of the null-stream technique (see also the study by Ajith *et al.* [30]).

A first improvement is to optimize the algorithm for implementing our test. An optimal identification of the integration time and frequency band over which the null and incoherent energies are calculated will improve the effectiveness of the test by minimizing the amount of noise included.

An important augmentation of the coherent analysis is improved techniques for determining the sky location of the source. Current efforts estimate the sky position as the extremum in a sky map of the null stream or some likelihood statistic [13, 20]. For example, Güsel and Tinto [13] demonstrated that locating the minimum of the null energy allows one to determine the direction to the source of a kiloHertz GWB with high accuracy for typical SNRs of $\sim 40 - 60$ (converted to our ρ_{rms}). However, as we have seen, sky maps exhibit structure which is a combination of the network geometry and the signal waveform. For example, linearly polarized signals pro-

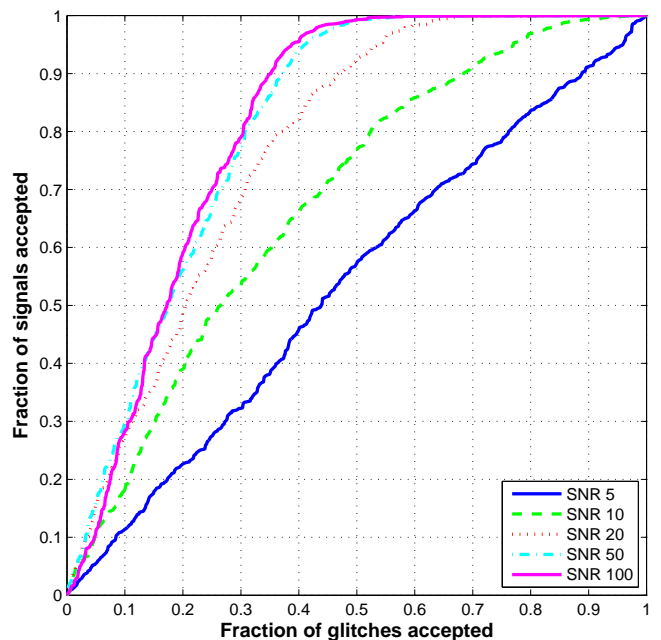


FIG. 11: Receiver-Operator Characteristic (ROC) plot for $\min(E_{\text{null}})$ as a statistic for distinguishing GWBs from noise glitches. The ROC curve value is given by the fraction of GWBs (true acceptance) and glitches (false acceptance) of given rms SNR falling to the left of a line of constant E_{null} (a vertical line) in Fig. 8. The lower slope of the curves at low acceptance is due to the fact that many glitches have sky positions for which the null energy is small, even when the SNR of the glitch is high. The null energy alone is therefore not very effective for confidently distinguishing GWBs from noise glitches. While one could choose a threshold that varies with E_{inc} to get better performance, $\min(E_{\text{null}})$ is still not as powerful a statistic as $\min(E_{\text{null}}/E_{\text{inc}})$.

duce interference fringes in the sky map. These fringes appear as rings of fixed time delay with respect to the various detector baselines. A global analysis which takes account of this structure could in principle average over local noise fluctuations in the sky map to achieve an improved pointing accuracy for weaker signals.

We will further investigate Bayesian interpretations and formulations of the null-stream technique, and compare the effectiveness of this approach against the procedure presented in this work. We will also investigate the possibility of incorporating additional tests such as distribution-free (non-parametric) correlation tests. These could prove valuable when analyzing real data since they enforce known statistics even when the noise in the data follows an arbitrary noise distribution function.

APPENDIX A: NULL STREAM PROJECTION OPERATOR

In this section we derive explicit expressions for the projection operator which acts on the network data vec-

tor to produce null streams. This projection operator projects the data orthogonally to \mathbf{F}_w^+ and \mathbf{F}_w^\times .

Let \mathbf{m} and \mathbf{n} be any orthonormal pair of vectors that span the space spanned by \mathbf{F}_w^+ and \mathbf{F}_w^\times (the vectors \mathbf{F}_w^+ and \mathbf{F}_w^\times are not necessarily orthogonal). Then the projection operator that removes the gravitational-wave contribution is

$$P_{\alpha\gamma}^{\text{NS}} = \sum_{\beta=1}^D (\delta_{\alpha\beta} - m_\alpha m_\beta) (\delta_{\beta\gamma} - n_\beta n_\gamma). \quad (\text{A1})$$

For example, choosing

$$\mathbf{m} = \frac{\mathbf{F}_w^+}{|\mathbf{F}_w^+|}, \quad (\text{A2})$$

$$\mathbf{n} = \frac{\mathbf{F}_w^\times - (\mathbf{m} \cdot \mathbf{F}_w^\times) \mathbf{m}}{|\mathbf{F}_w^\times - (\mathbf{m} \cdot \mathbf{F}_w^\times) \mathbf{m}|}, \quad (\text{A3})$$

one finds

$$P_{\alpha\gamma}^{\text{NS}} = \delta_{\alpha\gamma} - \frac{1}{\det(M)} \begin{bmatrix} F_{w\alpha}^+ & F_{w\alpha}^\times \\ F_{w\alpha}^\times & F_{w\alpha}^+ \end{bmatrix} \begin{bmatrix} M_{\times\times} & -M_{+\times} \\ -M_{+\times} & M_{++} \end{bmatrix} \begin{bmatrix} F_{w\gamma}^+ \\ F_{w\gamma}^\times \end{bmatrix} \quad (\text{A4})$$

where the 2×2 matrix M is defined by

$$\mathbf{M} = \mathbf{F}_w^T \mathbf{F}_w. \quad (\text{A5})$$

In matrix notation (A4) becomes

$$\mathbf{P}^{\text{NS}} = \mathbf{I} - \mathbf{F}_w \mathbf{M}^{-1} \mathbf{F}_w^T, \quad (\text{A6})$$

If $\mathbf{F}_w^+ \propto \mathbf{F}_w^\times$ (e.g., for co-aligned detectors) then the projection operator simplifies to

$$P_{\alpha\beta}^{\text{NS}} = (\delta_{\alpha\beta} - m_\alpha m_\beta) \quad (\text{A7})$$

with m_α given by (A2).

APPENDIX B: MINIMUM-VARIANCE WAVEFORM RECONSTRUCTION

In this section we derive explicit expressions for the two amplitude components of the wave, h_+ and h_\times , as optimally reconstructed as linear combinations of the detector data. This is a generalization of the technique used by Gürsel and Tinto [13], and was first derived by Flanagan and Hughes [6].

We will assume that the whitened data streams have been time-shifted before these combinations are constructed, and will simply write $\tilde{d}_{w\alpha}[f_i]$ for $\tilde{d}_{w\alpha}[f_i] e^{i2\pi f_i \Delta t_\alpha(\theta, \phi)}$, $\alpha = 1, \dots, D$.

Our goal can be reduced to the problem of identifying two vectors \mathbf{V}_+ , \mathbf{V}_\times such that

$$\tilde{h}_+^{\text{est}} \equiv \mathbf{V}_+ \cdot \tilde{\mathbf{d}}_w = \tilde{h}_+ + \mathbf{V}_+ \cdot \tilde{\mathbf{n}}_w \quad (\text{B1})$$

$$\tilde{h}_\times^{\text{est}} \equiv \mathbf{V}_\times \cdot \tilde{\mathbf{d}}_w = \tilde{h}_\times + \mathbf{V}_\times \cdot \tilde{\mathbf{n}}_w. \quad (\text{B2})$$

From the above equations we conclude that these two vectors must satisfy the constraints

$$\begin{aligned} \mathbf{V}_+ \cdot \mathbf{F}_w^+ &= 1 \\ \mathbf{V}_+ \cdot \mathbf{F}_w^\times &= 0 \\ \mathbf{V}_\times \cdot \mathbf{F}_w^+ &= 0 \\ \mathbf{V}_\times \cdot \mathbf{F}_w^\times &= 1. \end{aligned} \quad (\text{B3})$$

This implies that the errors in estimating the two waveforms are

$$\delta \tilde{h}_+^{\text{est}} = \tilde{h}_+^{\text{est}} - \tilde{h}_+ = \mathbf{V}_+ \cdot \tilde{\mathbf{n}}_w \quad (\text{B4})$$

$$\delta \tilde{h}_\times^{\text{est}} = \tilde{h}_\times^{\text{est}} - \tilde{h}_\times = \mathbf{V}_\times \cdot \tilde{\mathbf{n}}_w. \quad (\text{B5})$$

If the noises affecting the detectors are Gaussian distributed, the ‘‘optimal’’ choice for \mathbf{V}_+ , \mathbf{V}_\times is that implied by minimizing the mean-square errors of the noises affecting the two reconstructed waveforms,

$$\frac{1}{N} \sum_{k=0}^{N-1} |\delta \tilde{h}_+^{\text{est}}[k]|^2 = \sum_{\alpha=1}^D V_\alpha^{+2}, \quad (\text{B6})$$

$$\frac{1}{N} \sum_{k=0}^{N-1} |\delta \tilde{h}_\times^{\text{est}}[k]|^2 = \sum_{\alpha=1}^D V_\alpha^{\times 2}. \quad (\text{B7})$$

That is, we want the shortest (in the Cartesian sense) vectors \mathbf{V}_+ , \mathbf{V}_\times which satisfy the constraints (B3). This minimization can be performed by using the method of the Lagrange multipliers. For instance, for \mathbf{V}_+ we have

$$\begin{aligned} 0 &= \frac{\delta}{\delta V_\alpha^+} \left[\sum_\beta V_\beta^{+2} + \lambda_+ \left(\sum_\beta V_\beta^+ F_{w\beta}^+ - 1 \right) \right. \\ &\quad \left. + \lambda_\times \left(\sum_\beta V_\beta^+ F_{w\beta}^\times \right) \right], \end{aligned} \quad (\text{B8})$$

where $(\lambda_+, \lambda_\times)$ are the two Lagrange multipliers. The above equation leads to

$$V_\alpha^+ = -\frac{1}{2} (\lambda_+ F_{w\alpha}^+ + \lambda_\times F_{w\alpha}^\times). \quad (\text{B9})$$

Imposing the constraints (B3) in the above equation results in the linear system of equations

$$\begin{pmatrix} -2 \\ 0 \end{pmatrix} = M \begin{pmatrix} \lambda_+ \\ \lambda_\times \end{pmatrix}, \quad (\text{B10})$$

where the symmetric 2×2 matrix M is defined in (A5). Inverting \mathbf{M} , it follows that

$$\begin{pmatrix} \lambda_+ \\ \lambda_\times \end{pmatrix} = \frac{2}{\det(M)} \begin{pmatrix} -M_{\times\times} \\ M_{+\times} \end{pmatrix}, \quad (\text{B11})$$

which gives

$$V_\alpha^+ = \frac{1}{\det(M)} (F_{w\alpha}^+ M_{\times\times} - F_{w\alpha}^\times M_{+\times}). \quad (\text{B12})$$

By performing an analogous calculation for V_α^\times we find

$$V_\alpha^\times = \frac{1}{\det(M)} (-F_{w\alpha}^+ M_{+\times} + F_{w\alpha}^\times M_{++}). \quad (\text{B13})$$

Note that the weighting of a particular detector d_α vanishes if $F_{w\alpha}^+ = 0 = F_{w\alpha}^\times$, which occurs if detector d_α has no sensitivity to the sky location being considered ($F_\alpha^+ = 0 = F_\alpha^\times$), or if it is much noisier than the other detectors ($S_\alpha \rightarrow \infty$). In these cases, the expressions (B12,B13) at that frequency and sky position reduce to those for the network that does not include detector α .

In matrix form, $V_\alpha^{+, \times}$ are the rows of a $2 \times D$ matrix \mathbf{V} where from (B12), (B13), and (A5)

$$\mathbf{V} = \mathbf{M}^{-1} \mathbf{F}^T = (\mathbf{F}^T \mathbf{F})^{-1} \mathbf{F}^T. \quad (\text{B14})$$

That is, the waveform reconstruction matrix \mathbf{V} is the *pseudo-inverse* of \mathbf{F} [31]. Indeed, it is easily verified that

$$\mathbf{V} \mathbf{F} = \mathbf{I}. \quad (\text{B15})$$

This is equivalent to the conditions (B3).

If $\mathbf{F}_w^+ \propto \mathbf{F}_w^\times$ (e.g., for co-aligned detectors) then only a single linear combination of the two polarizations $h_{+, \times}$ can be extracted. Choosing the polarization gauge ψ' such that $|\mathbf{F}_w'^+| = (|\mathbf{F}_w^+|^2 + |\mathbf{F}_w^\times|^2)^{1/2}$, $\mathbf{F}_w'^\times = 0$, the reconstruction matrix reduces to simply

$$\mathbf{V} = \frac{\mathbf{F}_w'^+{}^T}{|\mathbf{F}_w'^+|^2}. \quad (\text{B16})$$

See Rakhmanov [31] for a discussion of singularities in waveform reconstruction due to rank-deficiency of \mathbf{F}_w , and the use of Tikhonov regularization to avoid such problems. Rakhmanov's expressions correspond to ours with the replacement $F_\alpha^{+, \times} \rightarrow F_{w\alpha}^{+, \times}$; i.e., replacing the antenna responses by the noise-weighted antenna responses.

ACKNOWLEDGMENTS

This work was performed under partial funding from the following NSF Grants: PHY-0107417, 0140369, 0239735, 0244902, 0300609, and INT-0138459. A. Searle was supported by the Australian Research Council and the LIGO Visitors Program. L. Stein was supported in part by an NSF REU Site grant. Simulations were performed on the Australian Partnership for Advanced Computing's National Facility under the Merit Allocation Scheme. For M. Tinto, the research was also performed at the Jet Propulsion Laboratory, California Institute of Technology, under contract with the National Aeronautics and Space Administration. This document has been assigned LIGO Laboratory document number LIGO-P060009-01-E.

-
- [1] <http://www.ligo.caltech.edu/>.
[2] <http://www.geo600.uni-hannover.de/>.
[3] <http://tamago.mtk.nao.ac.jp/>.
[4] <http://www.virgo.infn.it/>.
[5] E. E. Flanagan and S. A. Hughes, Phys. Rev. D **57**, 4535 (1998).
[6] E. E. Flanagan and S. A. Hughes, Phys. Rev. D **57**, 4566 (1998).
[7] F. Pretorius, Phys. Rev. Lett. **95**, 121101 (2005).
[8] T. Zwerger and E. Muller, Astron. Astrophys. **320**, 209 (1997).
[9] H. Dimmelmeier, J. Font, and E. Muller, Astron. Astrophys. **393**, 523 (2002).
[10] C. Ott, A. Burrows, E. Livne, and R. Walder, Astrophys. J. **600**, 834 (2004).
[11] M. Shibata and Y. I. Sekiguchi, Phys. Rev. D **69**, 084024 (2004).
[12] P. Mészáros, Ann. Rev. Astron. Astrophys. **40**, 137 (2002).
[13] Y. Gursel and M. Tinto, Phys. Rev. D **40**, 3884 (1989).
[14] M. Tinto, J. W. Armstrong, and F. B. Estabrook, Phys. Rev. D **63**, 021101(R) (2000).
[15] M. Tinto and S. L. Larson, Phys. Rev. D **70**, 062002 (2004).
[16] L. Wen and B. Schutz, Class. Quantum Grav. **22**, S1321 (2005).
[17] G. Strang, *Introduction to Linear Algebra, 3rd Edition* (Wellesley-Cambridge Press, 1998).
[18] S. Chatterji, L. Blackburn, G. Martin, and E. Katsavounidis, Class. Quant. Grav. **21**, S1809 (2004).
[19] S. Chatterji, PhD dissertation, MIT (2004).
[20] S. Klimentenko, S. Mohanty, M. Rakhmanov, and G. Mitselmakher, Phys. Rev. D **72**, 122002 (2005).
[21] M. Tinto, in *Proceedings of the International Conference on Gravitational Waves: Source and Detectors*. (World Scientific (Singapore), 1996).
[22] W. G. Anderson, P. R. Brady, J. D. E. Creighton, and E. E. Flanagan, Phys. Rev. D **63**, 042003 (2001).
[23] A. Dietz, J. Garofoli, G. Gonzalez, M. Landry, B. O'Reilly, and M. Sung, LIGO Document: LIGO-T050262-D (2005).
[24] <http://www.lsc-group.phys.uwm.edu/cgi-bin/cvs/viewcvs.cgi/m>
[25] <http://www.ligo.caltech.edu/docs/T/T970130-F.pdf>.
[26] W. Althouse et al., Rev. Sci. Instrum. **72**, 3086 (2001).
[27] F. Beauville et al., To appear in the proceedings of 6th Edoardo Amaldi Conference on Gravitational Waves (2005), gr-qc/0509041.
[28] http://www.ligo.caltech.edu/~lazz/distribution/LSC_Data/.
[29] A. Lazzarini, S. Bose, P. Fritschel, M. McHugh, T. Regimbau, K. Reilly, J. D. Romano, J. T. Whelan,

- S. Whitcomb, and B. F. Whiting, Phys. Rev. D **70**, 062001 (2004).
- [30] P. Ajith, M. Hewitson, L. Wen, and I. S. Heng, LIGO-T050167-00-Z (2005).
- [31] M. Rakhmanov, LIGO Document: LIGO-P060005 (2006).
- [32] Any gravitational wave at the Earth, produced by a source at astronomical distances, can be regarded as a plane wave.
- [33] The null space of \mathbf{F}_w^T is the set of all vectors \mathbf{x} such that $\mathbf{F}_w^T \mathbf{x} = 0$.
- [34] XPIPELINE can also process multiple frequency bands; we use a single band in this demonstration for simplicity.